Available online at www.sciencedirect.com
SCIENCE DIRECT
Journal of Power Sources 152 (2005) 146–155
JOURNAL OF POWER SOURCES
www.elsevier.com/locate/jpowsour

Corrosion studies of a copper–beryllium alloy in a simulated polymer electrolyte membrane fuel cell environment

Vaibhav V. Nikam, Ramana G. Reddy *

Department of Metallurgical and Materials Engineering, Center for Green Manufacturing, The University of Alabama, Tuscaloosa, AL 35487-0202, USA

Received 17 January 2005; accepted 18 February 2005
Available online 13 April 2005

Abstract

Bipolar plates play an important role in the performance, and cost of fuel cell. The properties of copper–beryllium alloy were studied in simulated fuel cell environment. Corrosion studies of the alloy were carried out by using Tafel extrapolation, and potentiodynamic polarization plots at various temperatures. The conditions selected were 0.5 M H_2SO_4 with varying pH in the range of 3–5 and 5% (v/v) HCl + 5% (v/v) Na_2SO_4 with the bubbling of oxygen, and argon. The corrosion rate for the alloy was found to be 0.05, and 0.28 μm year^{-1} at 25 and 70 °C, respectively. A similar range of corrosion rates was reported in literature for other copper alloys. Due to their good corrosion resistance and high conductivity the alloy can be considered as a candidate material for bipolar plates. Use of copper alloy in bipolar plate will reduce the contact resistance in cell stack due to their high conductivity.

Keywords: PEM fuel cell; Corrosion; Tafel extrapolation; Copper–beryllium alloys

1. Introduction

A fuel cell is an energy conversion device. It is an electrochemical device that converts chemical energy of fuel and oxidant into electricity. A fuel cell usually consumes chemicals, which are supplied in the form of hydrogen and oxygen to produce the electricity and thus are not exhaustible like batteries. Fuel cells find applications in vehicles, space shuttles, and various areas where electricity is needed [1].

A fuel cell is essentially an electrochemical cell consisting of two electrodes, namely anode and cathode. Hydrogen or another gaseous fuel is continuously fed to a porous anode and oxygen is continuously fed to the surface of a porous cathode. Electrochemical oxidation of the fuel takes place while oxygen is electrochemically reduced [2]. This reaction gives rise to a flow of electrons through the outer load and a flow of the ions (protons) through the electrolyte as shown in Fig. 1.

The two half cell reactions in the fuel cell are given by:

$$\text{Anode}: \ H_2 \rightarrow 2H^+ + 2e^- \quad E^0 : 0\,\text{V}$$

$$\text{Cathode}: \ \tfrac{1}{2}O_2 + 2H^+ + 2e^- \rightarrow H_2O \quad E^0 : 1.229\,\text{V}$$

The overall reaction is thus

$$H_2 + \tfrac{1}{2}O_2 \rightarrow H_2O \quad E^0 : 1.229\,\text{V}$$

The fuel cell is an environmental friendly device since the only by-product of the cell reaction is water.

The bipolar plate is one of the most important components of the PEM fuel cell. It separates the individual cells in the stack. The main function of the bipolar plate is to provide a conduct for hydrogen and oxidant flow. It accounts for approximately 80% of the weight of fuel cell. Due to the critical machining requirement for gas flow fields, the bipolar plates contribute approximately 15% of the total cost of stack components [3]. Earlier various materials like graphite, SS316, molded composites were proposed and used as the bipolar plate material [4–6].

* Corresponding author. Tel.: +1 205 348 1740; fax: +1 205 348 2164.
E-mail address: rreddy@coe.eng.ua.edu (R.G. Reddy).

0378-7753/$ – see front matter © 2005 Elsevier B.V. All rights reserved.
doi:10.1016/j.jpowsour.2005.02.035

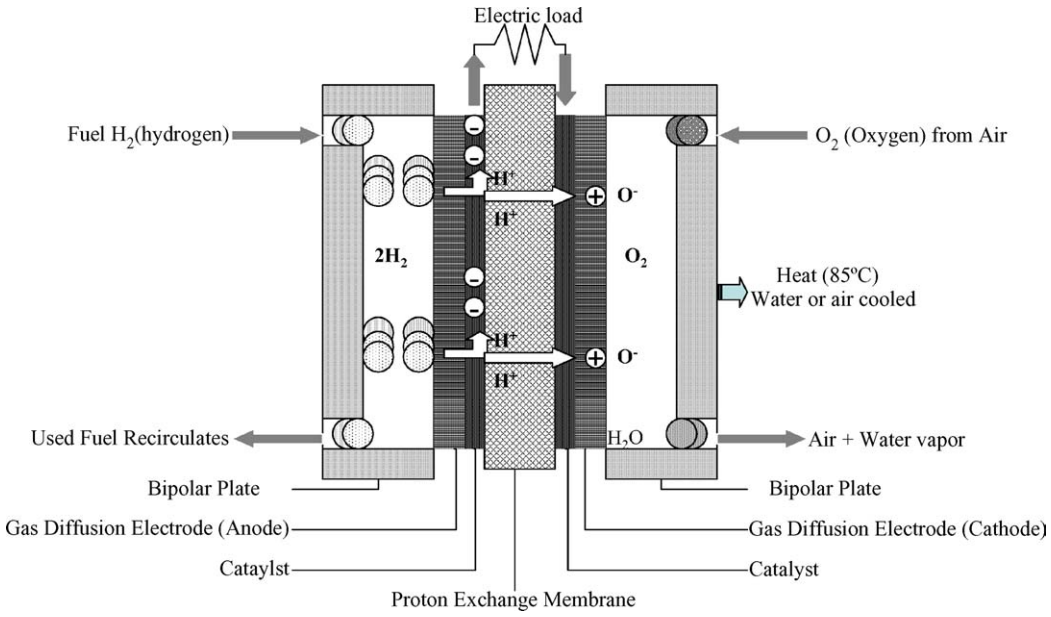

Fig. 1. Schematic diagram of the PEM fuel cell.

Several researchers have reported that the PEM fuel cell functions in an acidic environment (pH 3.0–5.0) due to presence of SO_4^{2-}, Cl^-, F^-, etc. ions in the Nafion® membrane [7,8]. The material for bipolar plate application must have good corrosion resistance and conductivity to reduce resistive losses in the acidic environment. Copper and copper alloys are well known for their good electrical and thermal conductivity. Copper–beryllium alloy (C-17200) was considered in this study because of its good conductivity, oxidation resistance, and corrosion resistance.

The corrosion behavior of copper–beryllium alloy (C-17200) in a fuel cell environment was studied using electrochemical techniques. The experimental data is essential for understanding and modifying corrosion behavior of materials in fuel cell.

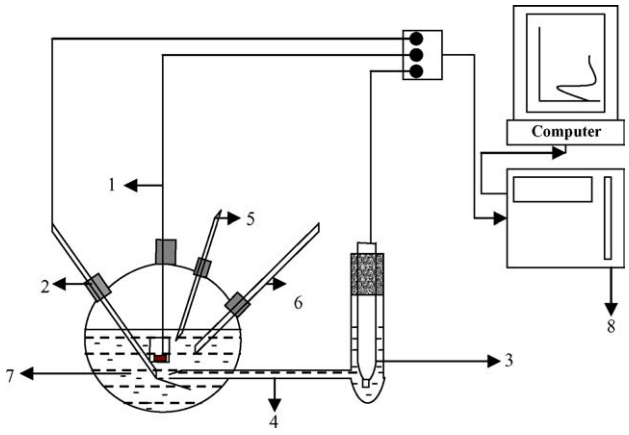

Fig. 2. Electrochemical cell: (1) working electrode, (2) counter electrode, (3) saturated calomel electrode, (4) luggin capillary, (5) gas bubbling tube, (6) thermometer, (7) 0.5 M H_2SO_4 solution, and (8) potentiostat.

2. Experimental procedure for corrosion experiments

The electrochemical experiments were carried out in a simple cell consisting of a three-electrode arrangement with a working electrode, auxiliary electrode, and a reference electrode as shown in Fig. 2. The counter electrode was platinum foil spot welded to platinum wire sealed in Pyrex, and Accumet™ saturated calomel reference electrode was fixed in the separable funnel outside the cell. The funnel was filled with saturated KCl solution. The sealed funnel was carefully attached to the cell without contaminating the cell. As reported in literature, several electrolytes were used to conduct electrochemical studies replicating the fuel cell environment [7,8]. In this research, we studied two such electrolytes, viz. 0.5 M H_2SO_4, and 5% (v/v) HCl + 5% (v/v) Na_2SO_4. The sample was then placed just above the tip of the Luggin capillary (approximately 2–3 mm). The tests were conducted using a potentiostat Model 273 A by EG&G Princeton Applied Research and analyzed with EG&G Version 2.0.1 corrosion software [9]. The working electrode was prepared by accurately cutting 10 mm × 10 mm × 0.8 mm dimensions of C-17200 plate obtained from Alfa Aesar. The composition of C-17200 alloy was Be 1.8–2.0%, Ni + Co 0.2%, Ni + Co + Fe 0.6%, Al 0.2%, Si 0.2% and copper as the balance (weight percent). Electrical contact was made by using single stranded copper wire with silver conducting paint. The samples thus prepared were mounted in an epoxy mould carefully exposing 10 mm × 10 mm surface to the electrolyte. The mounted samples were ground with 240-grit emery paper. The polishing was further carried sequentially with 400, 600, 800, 1000, and 1200 grit emery papers. Wet polishing

with water as media was carried out. The samples were degreased by using acetone, washed with distilled water and dried just before testing. Sample preparation and cleaning was followed as per ASTM standard: G1-03 [10,11]. The cell was calibrated with pure copper and SS-316 and corrosion rates were found to be consistent with reported values [7,9]. The electrochemical cell was heated with an automatic temperature controlled hotplate (accuracy ±1 °C). The experiments were performed at 25, 50, 60, and 70 °C, in both oxidizing and non-oxidizing atmospheres. Air was used as the bubbling gas in the oxidizing environment and bubbling was carried out for 1 h before the start of experiments. Similarly, argon was used as the bubbling gas in the non-oxidizing atmosphere. The corrosion current was determined by the Tafel extrapolation method. The scans were carried out in both positive and negative directions. The scan rate was 10 mV s^{-1}, with a scan increment of 1 and 2 mV s^{-1}. Initial and final potentials were chosen as per the open-circuit potential to cover both anodic and cathodic branches [9]. The stabilization time for each test was 3 h before starting experiment. After corrosion testing the samples were characterized using scanning electron microscopy (SEM) with EDS attachment, X-ray diffractometer (XRD) and X-ray photo-electron spectroscopy (XPS) techniques to investigate the corrosion products.

3. Results of electrochemical experiments

3.1. Tafel extrapolation results

3.1.1. Experiments in 0.5 M H_2SO_4 electrolyte environment

Tafel extrapolation plots for various conditions in 0.5 M H_2SO_4 are presented in Figs. 3–7.

3.1.1.1. Experiments in non-oxidizing environment. Fig. 3 shows the Tafel extrapolation plots for C-17200 alloy in 0.5 M H_2SO_4 with pH 3.26, 4.08, and 5.17 at 25 °C in non-oxidizing atmosphere. The corrosion current in this case did not vary with large magnitude with pH, though it was observed that the corrosion current I_{corr} was increasing with increasing pH. The anodic curve was not showing remarkable active passive transition features in all plots except a hump like feature at approximately +0.3 V.

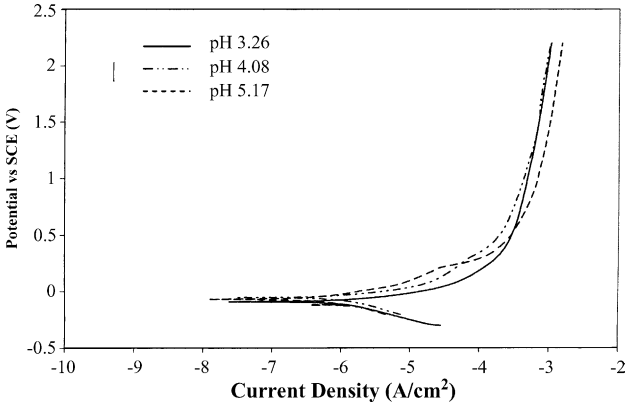

Fig. 3. Tafel extrapolation plots for C-17200 alloy in 0.5 M H_2SO_4 with pH 3.26, 4.08, and 5.17 at 25 °C under non-oxidizing conditions.

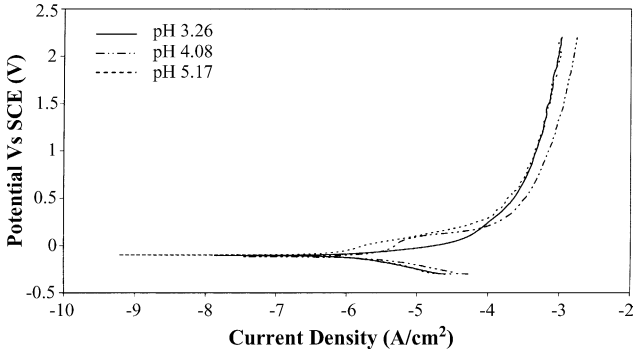

Fig. 4. Tafel extrapolation plots for C-17200 alloy in 0.5 M H_2SO_4 with pH 3.26, 4.08, and 5.17 at 25 °C under oxidizing conditions.

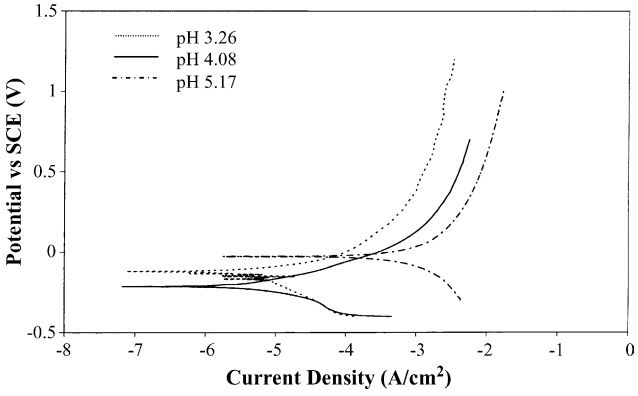

Fig. 5. Tafel extrapolation plots for C-17200 alloy in 0.5 M H_2SO_4 with pH 3.26, 4.08, and 5.17 at 50 °C under non-oxidizing conditions.

3.1.1.2. Experiments in oxidizing environment. Fig. 4 shows the Tafel extrapolation plots for C-17200 alloy in 0.5 M

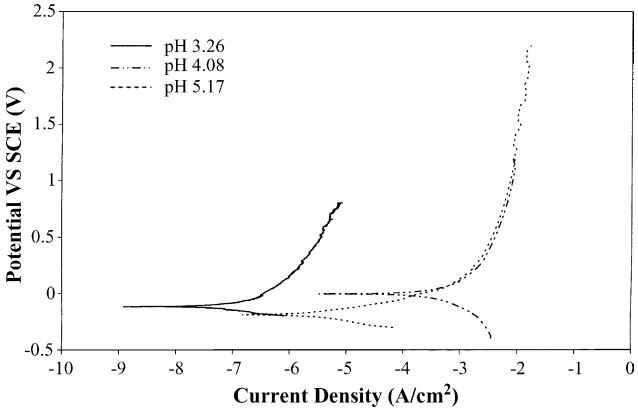

Fig. 6. Tafel extrapolation plot for C-17200 alloy in 0.5 M H_2SO_4 with pH 3.26, 4.08, and 5.17 at 60 °C under non-oxidizing conditions.

H_2SO_4 with pH 3.26, 4.08, and 5.17 at 25 °C in oxidizing atmosphere. The plots were showing similar features to the non-oxidizing atmosphere, but the corrosion potentials can be clearly seen to be decreased (more negative), increasing the anodic corrosion [9] and thus corrosion rate. The corrosion current I_{corr} was increasing with pH as observed in the previous case. The corrosion rates in oxidizing and non-oxidizing environment were not showing significant differences and so a non-oxidizing atmosphere was selected for high temperature experiments.

3.1.1.3. Experiments at different temperatures in non-oxidizing atmosphere. At 50 °C the Tafel extrapolation plots for the C-17200 alloy in 0.5 M H_2SO_4 with pH 3.26, 4.08, and 5.17 in non-oxidizing atmosphere show countable differences in current and voltage, as shown in Fig. 5. Corrosion currents and potentials were higher as compared to 25 °C. Enhanced corrosion at the high temperature is clearly seen.

Fig. 6 shows Tafel extrapolation plots for C-17200 alloy in 0.5 M H_2SO_4 with pH 3.26, 4.08, and 5.17 at 60 °C in a non-oxidizing environment. The corrosion current was observed to be increasing when compared with same sample at 50 °C. The plots were distinctly different for different pH. The corrosion current for pH 4.08 was observed to be slightly higher than that of pH 5.17. This anomaly can be explained by a different type of microstructure of corrosion layer discussed later.

As seen from the Tafel extrapolation plots in Fig. 7, for the C-17200 alloy in 0.5 M H_2SO_4 with pH 3.26, 4.08, and 5.17 at 70 °C, the corrosion current was substantially increased. Good corrosion resistance of C-17200 was observed at pH 3.26 than other pH values. There was no appreciable difference in corrosion current for pH 4.08 and 5.17.

3.1.2. Experiments in 5% (v/v) HCl + 5% (v/v) Na_2SO_4 electrolyte environment

As discussed previously several electrolyte choices are available to simulate the corrosive environment. But to study the corrosion behavior of materials for PEMFC applications, 5% (v/v) HCl + 5% (v/v) Na_2SO_4 electrolyte close to the real conditions due to the presence of both Cl^- and SO_4^{2-} ions in the electrolyte was selected. The effect of F^- can be neglected due to a very low concentration of these ions. Also it must be mentioned that the anodic reaction is far more important for the fuel cell application, so only anodic curve of polarization experiments are reported here. As reported in the literature [8] the effect of pH for this electrolyte is not significant for copper and its alloys, and so the effect of pH was not studied in these experiments. The electrolyte was observed to have a pH of 1.7–1.9.

Fig. 8 shows the potentiodynamic polarization plots for the C-17200 alloy in 5% (v/v) HCl + 5% (v/v) Na_2SO_4 environment at various temperatures. Potentiodynamic polarization curves of C-17200 at various temperatures in the simulated atmosphere showed a similar trend in values though significantly different in anodic behavior than in the 0.5 M H_2SO_4 electrolyte.

The potentiodynamic behavior of the C-17200 alloy in the electrolyte at 25 °C showed anodic corrosion of the alloy increasing initially from −0.1 to 1.4 V. The plots clearly show a passivation region starting at approximately +0.3 V. This process is the active mechanism of corrosion at high temperatures. As seen from Fig. 8 the clear behavior of strong passivation was observed at this temperature. The corrosion current was observed to be slightly higher as compared to similar samples in 0.5 M H_2SO_4 electrolyte up to 60 °C.

As the test temperature is increased to 50 °C strong passivation is followed by a small activation curve as seen in Fig. 8. The start of the passivation region was observed to be shifted by approximately 0.1 V in the positive direction. Further increasing the temperature to 60 °C increased the rate of active corrosion but a shift of the passivation region was not observed. Above 0.8 V, the curve showed several active–passive regions.

At 70 °C, the first passivation is followed by a very strong activation region as shown in Fig. 8. The first passivation

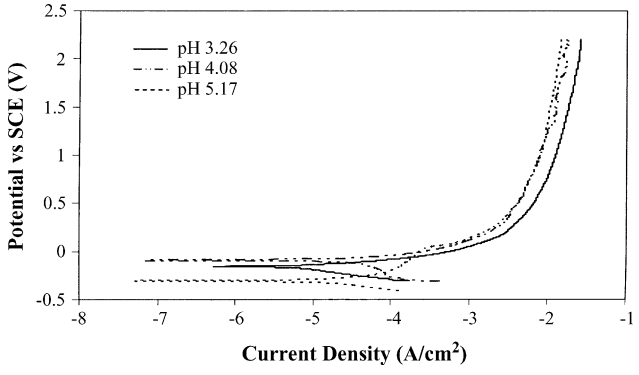

Fig. 7. Tafel extrapolation plot for C-17200 alloy in 0.5 M H_2SO_4 with pH 3.26, 4.08, and 5.17 at 70 °C under non-oxidizing conditions.

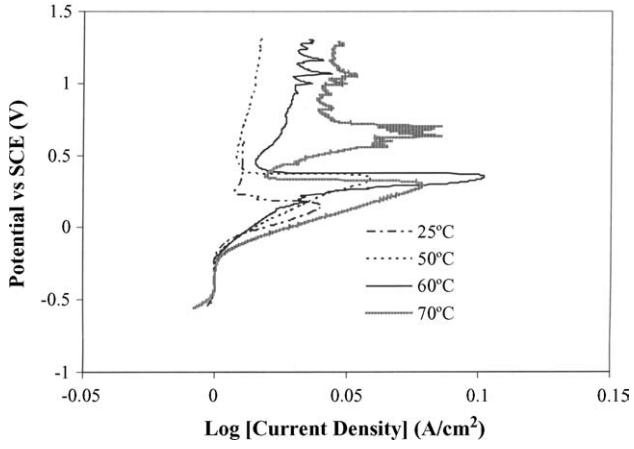

Fig. 8. Potantiodynamic polarization plots for C-17200 alloy in 5% (v/v) HCl + 5% (v/v) Na_2SO_4 at 25, 50, 60, and 70 °C under non-oxidizing conditions.

Table 1
Corrosion currents and potentials obtained from Tafel plots

Electrolyte	Non-oxidizing, 25 °C		Oxidizing, 25 °C		Non-oxidizing, 70 °C	
	Current ($\mu A\,cm^{-2}$)	Potential (V)	Current ($\mu A\,cm^{-2}$)	Potential (V)	Current ($\mu A\,cm^{-2}$)	Potential (V)
pH 3.26 (0.5 M H_2SO_4)	2.442	−0.009	4.203	−0.163	23.13	−0.25
pH 4.08 (0.5 M H_2SO_4)	2.622	−0.053	4.686	−0.115	23.4	−0.271
pH 5.17 (0.5 M H_2SO_4)	2.813	−0.051	4.894	−0.114	24.97	−0.373
5% HCl + 5% Na_2SO_4	3.905	−0.432	4.132	−0.441	22.015	−0.452

was observed to be shifted by approximately +0.15 V in going from 25 to 70 °C. After strong activation, the curve again showed a passive behavior followed by numerous small active–passive regions. The corrosion current was observed to increase with increasing temperature as expected.

The corrosion current and potential were obtained from the Tafel region of the polarization plot. The samples after corrosion testing were characterized by SEM, XRD and XPS techniques to study the nature of corrosion products.

3.2. Calculation of corrosion rates

The corrosion current is obtained from Tafel plots by extrapolating the applied current density from the anode and cathode branches of Tafel plots to the open-circuit potential. The corrosion rate is expressed by following equation [11]:

$$\text{C.R.} = \frac{3.27 \times i_{\text{corr}} \times W}{\rho \times 10^3} \quad (1)$$

where corrosion rate (C.R.) is in micrometers per year ($\mu m\,year^{-1}$), W the equivalent weight in grams, ρ is the density of the sample in gram per centimeter cube, i_{corr} is corrosion current density in microampere per centimeter square ($\mu A\,cm^{-2}$).

The equivalent weight for alloys was calculated by following formula [12].

$$W = \sum_{i=1}^{m} \frac{x_i \times M_i}{z_i} \quad (2)$$

Here x_i is the mass fraction, z_i the electrons exchanged and M_i is the atomic weight of the ith element. The equivalent weight of C-17200 was calculated to be 28.6097 [9]. The uniform corrosion rate for the sample was thus calculated by using Eq. (1) [9].

Each experiment was repeated four times to observe repeatability and average values are reported. The results from the Tafel plots are presented in Table 1 (results shown for 25 and 70 °C). Calculated corrosion rates are presented in Table 2. The corrosion rates were in the range of 0.0277–0.28 $\mu m\,year^{-1}$.

3.3. SEM analysis

The scanning electron microscopy analysis for all samples was carried out using Philips XL30 scanning electron microscope. The samples were carefully removed from the epoxy mould and standard samples for SEM were prepared. The composition of the corrosion products were confirmed by using a X-ray diffractometer and X-ray photo-electron spectroscopy.

3.3.1. Analysis of corrosion samples in 0.5 M H_2SO_4 electrolyte environment

The morphology of the corrosion layer is very important in analyzing the details of the corrosion process. The micrographs did not show any distinct effect of pH and so only the micrographs of the pH 4.08 condition are discussed. Fig. 9 shows a micrograph of C-17200 alloy in 0.5 M H_2SO_4, pH 4.08, with non-oxidizing bubbling at 25 °C. A corrosion layer without any porosity was observed. The layer formed was observed to be very thin (<10 μm). The corrosion layers observed in case of samples in the oxidizing atmosphere (Fig. 10) and the non-oxidizing atmosphere (Fig. 9) were similar in nature, showing a thin corrosion layer and small areas of material removed due to corrosion.

The layer was observed to be non-porous and adherent to the substrate. This is one of the desirable properties to reduce the corrosion rate due to hindrance of the further corrosion of the substrate material. The oxide layer was observed to increase with increasing temperature.

A SEM micrograph of the C-17200 sample at 50 °C for pH 4.08 in a non-oxidizing atmosphere is shown in Fig. 11. The micrograph clearly shows the formation of a tarnishing

Table 2
Corrosion rates for C-17200 alloy at different experimental conditions

Electrolyte	Corrosion rate ($\mu m\,year^{-1}$)		
	Non-oxidizing atmosphere 25 °C	Oxidizing atmosphere 25 °C	Non-oxidizing atmosphere 70 °C
pH 3.26 (0.5 M H_2SO_4)	0.0277	0.0476	0.262
pH 4.08 (0.5 M H_2SO_4)	0.0297	0.0530	0.2655
pH 5.17 (0.5 M H_2SO_4)	0.0319	0.05543	0.2829
5% (v/v) HCl + 5% (v/v) Na_2SO_4	0.0442	0.0468	0.2493

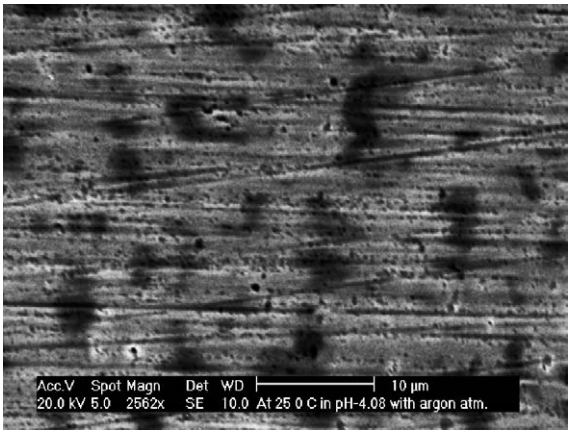

Fig. 9. SEM micrograph of C-17200 Tafel plot sample in pH 4.08 at 25 °C under a non-oxidizing atmosphere.

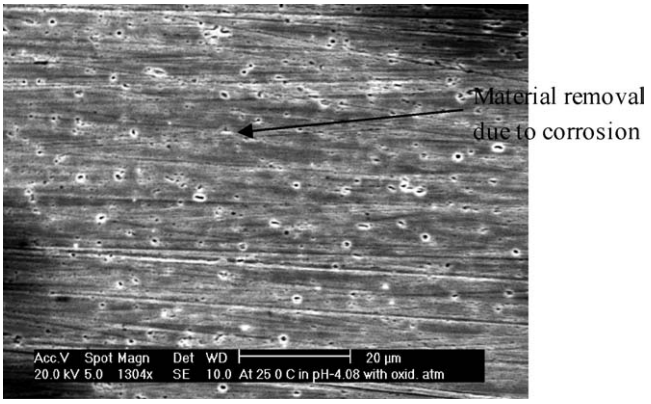

Fig. 10. SEM micrograph of C-17200 Tafel plot sample in pH 4.08 at 25 °C under an oxidizing atmosphere.

corrosion layer without porosity. SEM micrograph of C-17200 at 60 °C for pH 4.08 in non-oxidizing atmosphere is shown in Fig. 12. The micrograph in this case was observed to show a different morphology as compared to a similar sample at pH 3.26 and 5.17. The samples were observed to show layer flakes or blisters. This explains the high corrosion current and

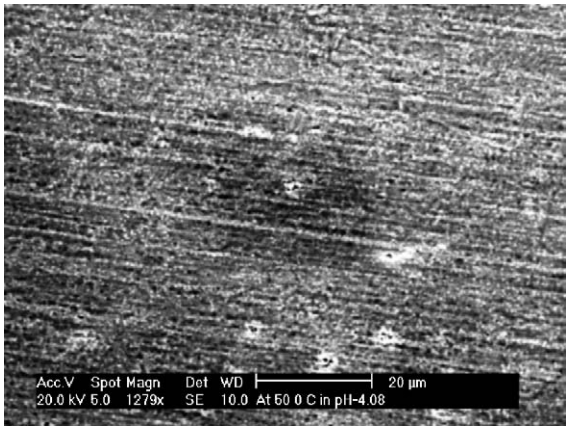

Fig. 11. SEM micrograph of C-17200 Tafel plot sample under pH 4.08 at 50 °C under a non-oxidizing atmosphere.

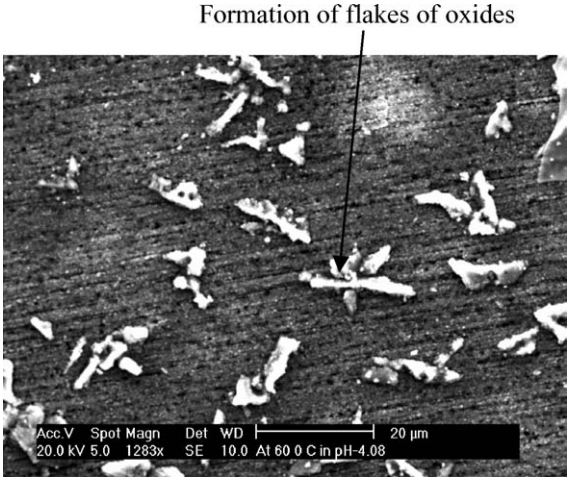

Fig. 12. SEM micrograph of Tafel plot sample in pH 4.08 at 60 °C under a non-oxidizing atmosphere.

potential for these samples as compared to pH 5.17. The blister formation is a typical characteristic of copper alloys like Cu–Ni alloys reported by researchers [13]. The XRD analysis of the corrosion layer revealed cuprous oxide (Cu_2O) as the major compound. The layer was observed to be firmly adherent to the substrate. Higher current recorded was due to bursting of blisters in some areas and divert exposure of the substrate material to corrode.

The corrosion layer for a C-17200 sample at 70 °C in a non-oxidizing atmosphere was observed to be non-porous, non-flaky as shown in Fig. 13. The layer was also observed to develop uniformly over the entire surface. The increase in the corrosion current, i.e. increase in corrosion rate with increasing temperature, revealed the enhanced formation of the corrosion layer.

3.3.2. Analysis of corrosion samples in 5% (v/v) HCl + 5% (v/v) Na_2SO_4

A SEM micrograph from the potentiodynamic polarization experiment in 5% (v/v) HCl + 5% (v/v) Na_2SO_4

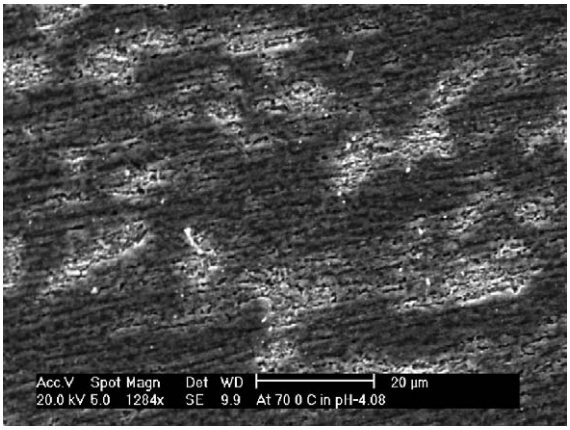

Fig. 13. SEM micrograph of Tafel plot Sample in pH 4.08 at 70 °C under a non-oxidizing atmosphere.

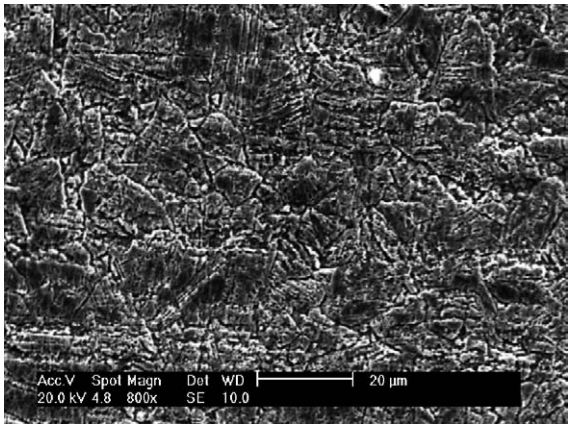

Fig. 14. SEM micrograph of C-17200 alloy from potentiodynamic polarization testing at 25 °C in 5% (v/v) Na_2SO_4 + 5% (v/v) HCl solution under non-oxidizing conditions.

electrolyte at 25 °C is shown in Fig. 14. The micrograph shows clear non-porous corrosion product layer. The layer was observed to be strongly adherent to the substrate. This tarnishing layer is due to the passivation observed. The corrosion products formed were observed to be insoluble in the electrolyte. A SEM micrograph from the potentiodynamic polarization experiment in 5% (v/v) Na_2SO_4 + 5% (v/v) HCl solution at 50 °C is shown in Fig. 15. The micrograph is similar in morphology to the 25 °C sample. Tarnishing layer of corrosion products was observed.

A SEM micrograph following the potentiodynamic polarization experiment in 5% (v/v) Na_2SO_4 + 5% (v/v) HCl solution at 60 °C is shown in Fig. 16. The micrograph shows several well-defined areas separated by a different microstructure. The well-defined area was designated as *A* and matrix was designated as *B*. Higher magnification of area *B* was similar to area *A* but was composed of several pores which contributed to several active–passive regions in the polarization plots (Fig. 8). EDS analysis of area *A* and *B* was carried out. Elemental composition of area *A* and *B* was

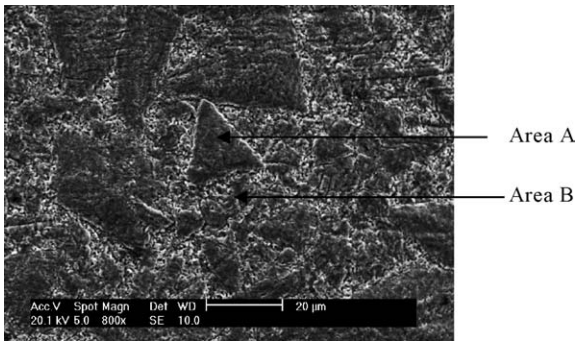

Fig. 16. SEM micrograph of C-17200 alloy from potentiodynamic polarization testing at 60 °C in 5% (v/v) Na_2SO_4 + 5% (v/v) HCl solution under non-oxidizing conditions.

observed to be the same (Cu: ∼36 at.%, Be: ∼62 at.%, O: ∼2 at.%). At high temperatures, the formation of porous areas may be favored.

Fig. 17 is a SEM micrograph from potentiodynamic polarization experiment in 5% (v/v) Na_2SO_4 + 5% (v/v) HCl solution at 70 °C. The micrograph is similar to Fig. 11 (60 °C). Thus, it can be concluded that a non-porous layer of corrosion product was formed on those samples, which contributed to protection of the alloy surface below it. XRD analysis was used for further investigation of corrosion product.

3.4. XRD analysis

XRD analysis of the samples after corrosion testing was carried out using a Philips XRG 2500 powder diffractometer. XRD spectra for samples at 25 and 70 °C in 0.5 M H_2SO_4 environment are shown in Fig. 18. The analysis showed a similar trend for all samples. The XRD spectrum was observed to show small intensity peaks due to a very thin corrosion layer. Major peaks of copper and cuprous oxide were observed which is consistent with the literature [14]. The graphs showed a gradual increase in peak intensity of

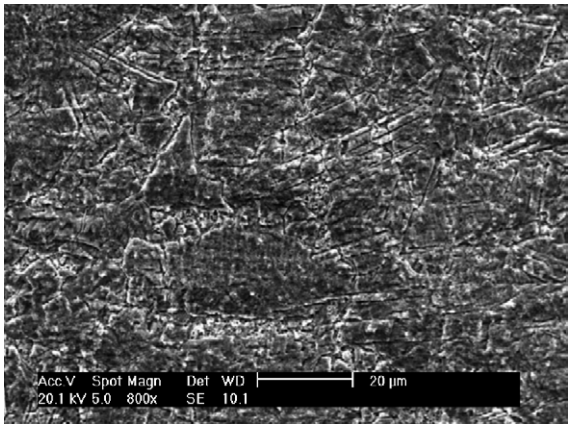

Fig. 15. SEM micrograph of C-17200 alloy from potentiodynamic polarization testing at 50 °C in 5% (v/v) Na_2SO_4 + 5% (v/v) HCl solution under non-oxidizing conditions.

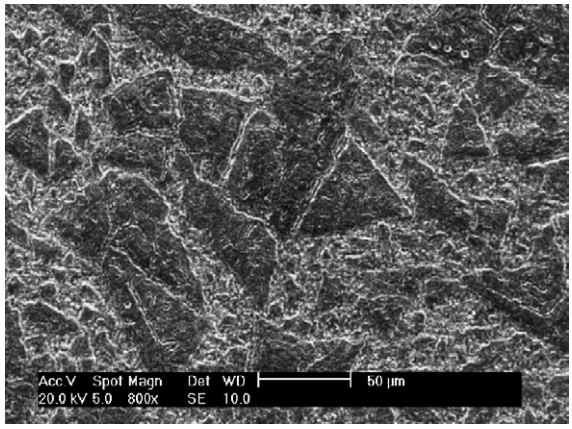

Fig. 17. SEM micrograph of C-17200 alloy from potentiodynamic polarization testing at 70 °C in 5% (v/v) Na_2SO_4 + 5% (v/v) HCl solution under non-oxidizing conditions.

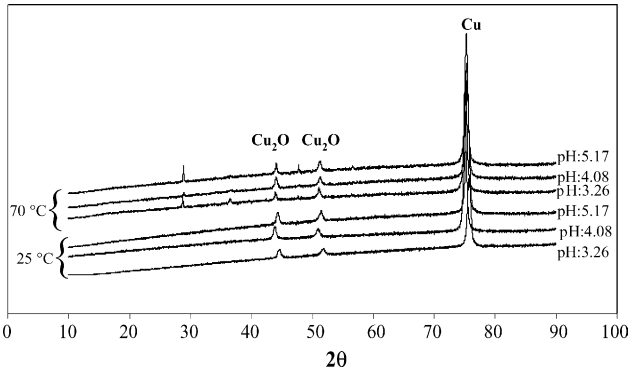

Fig. 18. XRD analysis of corrosion samples of C-17200 alloy in 0.5 M H_2SO_4.

cuprous oxide with temperature. Similarly, the intensity of cuprous oxide peaks was observed to increase with increasing pH, though not very significantly. This supports the view that the alloy is prone to corrosion and forms a layer of cuprous oxide at high pH and temperature. At lower pH, corrosion was less because of the formation of a thin, tarnish oxide film on the substrate. This clearly shows that the corrosion layer formed was composed of Cu_2O, i.e. cuprous oxide.

Though cuprous oxide is favored over cupric oxide, cupric oxide may also be formed under given conditions as reported in literature [15]. XPS analysis of corrosion samples was further carried to analyze the corrosion products below the surface.

3.5. XPS analysis

The corrosion samples were analyzed for XPS analysis using a Kratos XPS surface analyzer. Samples were mounted on standard sample holders, blasted with high pressure CO_2 to clean the surface from dust and other impurities. Cleaned samples were inserted into the sample transfer chamber for outgassing. Each sample was sputter cleaned using 4 kV Ar^+ ions for 2 min to remove surface contaminants before XPS analysis [9].

Survey and high resolution spectra were taken at 160 and 80 eV energies, respectively. The concentric hemispherical analyzer was operated in Fixed Analyzer Transmission and non-monochromatic mode. An Al Kα X-ray source was used for exciting the photoemission process. XPS spectra from corrosion samples of C-17200 in 0.5 M H_2SO_4 at pH 3.26, and 25, 50, 60, and 70 °C are shown in Fig. 19. XPS spectra of samples were similar even with increasing temperature. In the spectrum the Cu $2p_{3/2}$ peak is at 932.7 eV, which suggests that either or both elemental Cu (932.7 eV) or Cu_2O (932.5 eV) were present on the surface. Also Cu $2p_{3/2}$ peak is at 933.6 eV confirming oxides of copper. Thus, peaks of copper and cuprous oxide were showing the highest intensity. Also they were observed to overlap. The other major peak was at 952.7 eV for the Cu $2p_{1/2}$, peak, which is cupric oxide. This analysis clearly shows that cupric oxide and cuprous oxide are both present in the corrosion products [9].

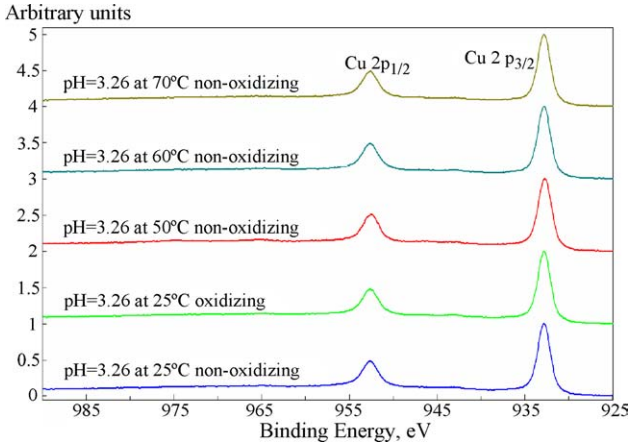

Fig. 19. XPS spectrum for corrosion samples of C-17200 in 0.5 M H_2SO_4 at pH 3.26 at 25, 50, 60, and 70 °C.

4. Discussion

The corrosion results for the C-17200 alloy were compared with corrosion properties of other copper and copper alloys. Several reports have discussed the behavior of copper and its alloys in an acidic environment. Some literature has reported the change in pH of the solution due to formation and consumption of H^+ ions [16], but due to very small span of experiment (<5 min for scan) this possibility can be neglected. Its long been known that copper and its alloys are prone to a higher corrosion rate with increasing pH [14,17]. This behavior is due to the increased formation of Cu_2O with high pH in acidic environment [14,17], which is consistent with experiments in 0.5 M H_2SO_4 as seen from Table 1 and the SEM micrographs of those experiments. The corrosion current was observed to be increasing with temperature due to the common enhancement of corrosion at high temperature. The dissolution of C-17200 alloy was observed to be similar to that of pure copper. The overall reaction is given below [18] (Eq. (3)) and thus the dissolution rate not only depends on the concentration of H^+ ion but also O_2. It was also reported that the concentration of SO_4^{2-} does not affect the corrosion rate [18].

$$Cu + O_2 + 2H^+ = Cu^{2+} + H_2O \quad (3)$$

Along with Cu_2O the formation of CuO was also reported [15]. Being nobler than H^+ in the electrochemical series the alloy exhibit following reaction (Eq. (4)) in the cathodic region apart from displacement of H^+ ions [15].

$$O_2 + 4H^+ + 4e^- = 2H_2O \quad (4)$$

Thus, O_2 produces CuO, which was observed as a duplex oxide layer evident from the XPS analysis. The formation of such a duplex layer of various copper oxides is reported

by several researchers [14,17]. Thus, the formation of duplex oxides in the 0.5 M H_2SO_4 environment can be explained by a similar type of stratification behavior reported in the literature for pure copper [17].

The dissolution of copper in HCl is similar to that of H_2SO_4. The initial reaction in the anodic region up to the first passivation is controlled by simple anodic reaction (Eq. (5)).

$$Cu = Cu^{2+} + 2e^{-} \quad (5)$$

The dissolution is controlled by the reaction given below (Eq. (6)) [15] after this region has passed i.e. after first passivation:

$$4Cu^{+} + O_2 + 4H^{+} = 4Cu^{2+} + 2H_2O \quad (6)$$

This increases the concentration of Cu^{2+} after passivation. Further, the current increases due to the reaction given below (Eq. (7)) [15]:

$$Cu + Cu^{2+} = 2Cu^{+} \quad (7)$$

More pronounced dissolution thus takes place after this. The several active–passive regions in the plot are due to the presence of porosity in the corrosion products discussed earlier. With increasing temperature the corrosion current was observed to be increasing as reported for the 0.5 M H_2SO_4 electrolyte.

US DOE have specified [19] that, for 5000 h life of PEMFC stack an acceptable corrosion rate is 16 $\mu A\,cm^{-2}$ or 95 $\mu m\,year^{-1}$. It is considered that 95% of the metallic ions, which account for corrosion of bipolar plate material, generated at this rate leave the cell stack along with by-product water. Thus, an acceptable corrosion rate can be calculated as [20]:

acceptable corrosion current

$$= \frac{16\,\mu A\,cm^{-2}}{1.00 - 0.95} = 320\,\mu A\,cm^{-2} \approx 0.3\,mA\,cm^{-2}$$

Thus the acceptable corrosion rate = 3.621 $\mu m\,year^{-1}$ for copper–beryllium alloy. The corrosion currents observed in both the electrolytes were well below this modified norm even at 70 °C as can be clearly seen from Table 2.

5. Conclusions

The experiments in the simulated fuel cell environment were carried out and the corrosion rates of the selected alloy at all experimental conditions were observed to be well within the DOE specified norm. The formation of a duplex type of oxide layer was observed to be formed as the corrosion product. The alloy tested can be considered as a candidate material for PEMFC bipolar/end plates. The corrosion resistance along with the high conductivity are the advantages of copper alloys over conventional bipolar plate materials. The implementation of copper alloys will assist in reducing the resistance losses in fuel cells.

Acknowledgments

Authors are very pleased to acknowledge the financial support given by US Department of Energy (DOE). The financial support given by Center for Advanced Vehicle Technology at the University of Alabama is also appreciated.

References

[1] Fuel Cell Handbook, fifth ed., West Virginia, EG&G Services, Parsons Inc., US Department of Energy, Office of Fossil Energy, National Energy Technology Laboratory, 2000.
[2] J. Larminie, A. Dicks, Fuel Cell Systems Explained, John Wiley & Sons Ltd., New York, 2000.
[3] J. Scholta, B. Rohland, V. Trapp, U. Focken, Investigation on novel low-cost graphite composite bipolar plates, J. Power Sources 84 (1999) 231–234.
[4] A. Kumar, R.G. Reddy, Effect of channel dimensions and shape in the flow-field distributor on the performance of the polymer electrolyte membrane fuel cells, J. Power Sources 113 (2003) 11–18.
[5] A. Kumar, R.G. Reddy, Modeling of a polymer electrolyte membrane fuel cell with metal foam in the flow-field of the bipolar/end plates, J. Power Sources 114 (2003) 54–62.
[6] A. Kumar, R.G. Reddy, Materials and design development for bipolar/end plate in fuel cells, J. Power Sources 129 (2004) 62–67.
[7] M. Li, S. Luo, C. Zeng, J. Shen, H. Lin, C. Cao, Corrosion behavior of TiN coated type 316 stainless steel in simulated PEMFC environments, Corros. Sci. 46 (2003) 1369–1380.
[8] S.-J. Lee, C.-H. Huang, Y.-P. Chen, Investigation of PVD coating on corrosion resistance of metallic bipolar plates in PEM fuel cell, J. Mater. Process. Technol. 140 (2003) 688–693.
[9] V.V.Nikam, Copper alloy bipolar/end plates in polymer electrolyte membrane fuel cells, Masters Thesis, The University of Alabama, Tuscaloosa, July 2004.
[10] ASTM standard G 3-89, Standard Practice for Conventions Applicable to Electrochemical Measurements in Corrosion Testing, ASTM publication, 03.02, 1997.
[11] R.G. Reddy, Z. Zhang, M.F. Arenas, D.M. Blake, Thermal stability and corrosivity evaluation of ionic liquids as thermal energy storage media, High Temp. Mater. Processes 22 (2003) 87–94.
[12] A.J. Denny, Principles and Prevention of Corrosion, second ed., Prentice-Hall Inc., Upper Saddle River, NJ, 1996, pp. 76–90.
[13] L. Shreir, Corrosion in Aqueous Solution in Corrosion, third ed., Butterworth-Heinemann, Oxford, 1994, pp. 1–92.
[14] S. Sathiyanarayanan, M. Sahre, W. Kautek, In-situ incidence X-ray diffractometry observation of pitting corrosion of copper in chloride solutions, Corros. Sci. 41 (1999) 1899–1909.
[15] A.M. Shams El Din, M.E. El Dahshan, A.M. Taj El Din, Dissolution of copper and copper–nickel alloys in aerated dilute HCl solutions, Desalination 130 (2000) 89–97.
[16] G. Bech-Nielsen, M. Jaskula, I. Chorkendorff, J. Larsen, The initial behavior of freshly etched copper in moderately acid, aerated chloride solutions, Electrochim. Acta 47 (2002) 4279–4290.
[17] G. Kear, B.D. Barker, F.C. Walsh, Electrochemical corrosion of unalloyed copper in chloride media—a critical review, Corros. Sci. 46 (2004) 109–135.

[18] R. Schumacher, A. Muller, W. Stockel, An in-situ study on the mechanism of the electrochemical dissolution of copper in oxygenated sulphuric acid, J. Electroanal. Chem. 219 (1987) 311–317.
[19] J. Neutzler, F. Barbi, Development of Advanced Low-Cost PEM Fuel Cell Stack and System Design for Operation on Reformate Used in Vehicle Power Systems, Report DE-FC02-97EE50476, Energy Partners Quarterly Report, 1999.
[20] R.L. Borup, N.E. Vanderborgh, Design and testing criteria for bipolar plate materials for PEM fuel cell applications, in: Materials Research Society Symposia Proceedings, 1995, pp. 151–155.